Study of hot tearing through ingot bending test: thermomechanical and solute transport analysis

Takao Koshikawa, Michel Bellet, Charles-André Gandin, Hideaki Yamamura, Manuel Bobadilla

SteelSim2013, 5th Int. Conf. on Modelling and Simulation of Metallurgical Processes in Steelmaking, Ostrava, September 10-12, 2013, DVD published by the Czech metallurgical Society (2013) 9 pages

Study of hot tearing through ingot bending test: thermomechanical and solute transport analysis

Takao Koshikawa[a,b], [a]MINES ParisTech & CNRS, CEMEF UMR 7635, 06904 Sophia Antipolis, France, [b]Nippon Steel & Sumitomo Metal Corporation, Personnel Division, 6-1, Marunouchi 2-chome, Chiyoda-ku, Tokyo, 100-8071, Japan, **Michel Bellet, Charles-André Gandin,** MINES ParisTech & CNRS, CEMEF UMR 7635, 06904 Sophia Antipolis, France, **Hideaki Yamamura,** Nippon Steel & Sumitomo Metal Corporation, Steelmaking R&D Division, 20-1 Shintomi, Futtsu City, Chiba Prefecture 293-8511, Japan, **Manuel Bobadilla**, ArcelorMittal Maizières, Research and Development, BP 30320 F-57283 Maizières-lès-Metz Cedex, France
takao.koshikawa@mines-paristech.fr

Hot tearing is one of the critical defects in cast products. It takes place close to the end of solidification, typically for solid fraction between 0.9 and 1.0, when the material is subjected to deformation based on tensile stress. In this study, a hot tearing experiment, so-called "bending test", is carried out in which a cast ingot is deformed by an external tool before the ingot is fully solidified. To analyze the experiment, two types of thermomechanical simulation are performed. The first one is a classical thermomechanical approach in which the mushy zone (composed of liquid and solid phases) is considered as a homogenized material so that a unique velocity field is solved for [1, 2]. Through stress-strain analyses, macroscopic hot tearing criteria found in literature are then evaluated [3]. The second type is an effective "two phase" modelling approach in which the liquid and solid velocity fields are computed separately in the mushy zone [4]. It allows simulating solute transport phenomena leading to macrosegregation induced by deformation shrinkage and advection. The effect of micro- and macro-segregation on hot tearing sensitivity is then discussed.

1. Introduction

Hot tearing is one of the critical defects in industrial casting processes such as continuous casting and ingot casting. It comes from a complicated combination of thermomechanical and solidification phenomena. This defect basically corresponds to the incapacity of liquid feeding in the presence of tensile stresses perpendicular to dendrite growth direction in a semi-solid zone. It develops when the solid fraction is typically between 0.9 and 1.0, called brittle temperature range (BTR). In this range, the ductility and strength of the alloy are decreased due to residual liquid film in between dendrites. A schematic summary of these phenomena is explained in reference [3].

In this study, the macroscopic hot tearing criterion of Won et al. [5] is evaluated, which is based on cumulated strain perpendicular to dendrite growth direction. The corresponding strain rate is denoted as $\hat{\dot{\varepsilon}}$, as explained in reference [3]. The strain based criterion is expressed as follows:

$$HCC_{WYSO} = \left(\int_{BTR} \hat{\dot{\varepsilon}} dt - \hat{\varepsilon}_C \right) \text{ with } \hat{\varepsilon}_C = \frac{\varphi}{\left(\hat{\dot{\varepsilon}}\right)^{m^*} BTR^{n^*}} \quad (1)$$

where $\hat{\varepsilon}_C$ is the strain limit and the three parameters are deduced by a non-linear data fitting with several hot tearing experiments: φ = 0.02821, m* = 0.3131, n* = 0.8638. It is obvious that, since BTR appears in the criterion, micro- and macro-segregation have an impact on the hot tearing sensitivity.

In order to identify hot tearing, a hot tearing experiment, so-called ingot bending test has been developed at Nippon Steel & Sumitomo Metal. For thermal mechanical analyses, two numerical codes are used, THERCAST and R2SOL developed at CEMEF. The micro- and macro-segregation effect on the hot tearing sensitivity is then discussed.

2. Ingot bending test

The schematic of the ingot bending test, is shown in Fig. 1. It has been designed to mimic real process thermomechanical solicitation; for instance, cooling rate and deformation. The procedure of the experiment is as follows: Molten metal is prepared in a ladle and the temperature is controlled as 1640 °C just before pouring. The molten metal is filled into the mould from the top through a tundish. The filling duration is about 70 sec. The mass of

metal is approximately 450 kg. The size of the ingot is 0.16 m thickness, 0.5 m width and 0.75 m height. After about 5 minutes from filling, the part of the mould (labeled as Right_mould_sup in Fig. 1) is removed. The ingot is then deformed during solidification by the external bending tool, located at the height of 0.45 m from the ingot bottom. The tool velocity and displacement are controlled and measured during the test. The test condition is summarized in Tab. 1, together with measured nominal compositions in the ladle before filling. To know temperature evolution during the test, thermocouples are positioned in the ingot and the left side mould (labeled as Left_mould in Fig. 1). Furthermore, the ingot surface temperature has been measured in case of trial N-4, using a pyrometer before and after deformation. After experiment, the ingot is cut at the ingot width center and the micrograph is investigated after appropriate etching to verify whether the specimen has hot tears or not.

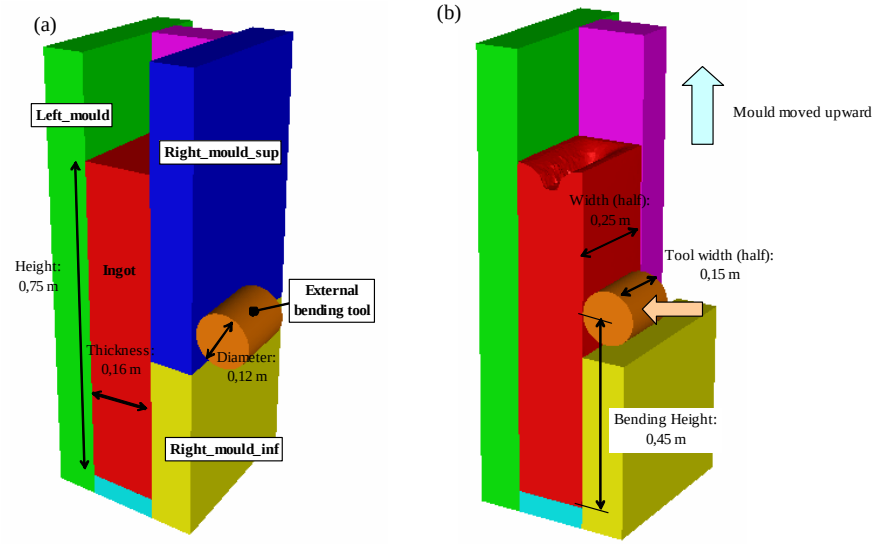

Fig. 1 Schematic of the hot tearing experiment developed at Nippon Steel & Sumitomo Metal: (a) initial state, (b) bending stage after mould removal. The shown configuration is a half of the setup, considering symmetry with respect to the width direction.

Tab. 1 Measured nominal compositions and experimental conditions

	Nominal compsition (mass%)						Mould removal	Bending start	Displacement	Velocity
	C	Si	Mn	P	S	Al	(s)	(s)	(mm)	(mm/s)
N-1	0,20	0,22	1,50	0,021	0,007	0,039	590	792	13	2,0
N-2	0,20	0,20	1,47	0,020	0,01	0,038	450	574	6	2,0
N-3	0,19	0,24	1,50	0,022	0,01	0,064	457	517	6	1,0
N-4	0,19	0,21	1,49	0,021	0,01	0,064	300	499	6	0,5
N-5	0,19	0,21	1,50	0,020	0,01	0,041	321	510	6	0,25

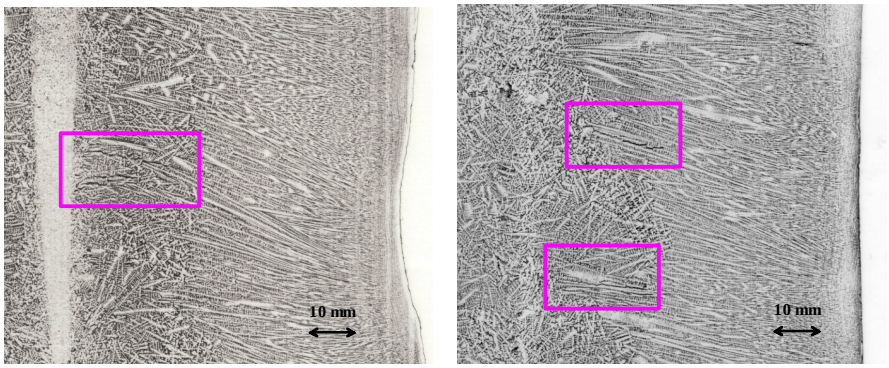

Fig. 2 Comparison of micrographs close to the bending region; trial N-1 (left) and N-4 (right). In both cases, there are hot tears indicated by pink square marks. In addition, a white band can be seen in N-1 (left), corresponding to less solute containing zone; negative macro-segregation

Fig. 2 shows two typical micrographs in case of N-1 and N-4 close to the bending region. In case of N-1, the surface deformation due to the bending tool is quite marked, while the micrograph of N-4 does not show much because of the difference of displacement. One can find dendritic microstructure which grows from the ingot surface (right hand side) toward the centre of the ingot (left hand side). Around the centre of the ingot, the morphology is changed to equiaxed

type, which is due to the decrease of cooling rate close to the core. In both cases, there are hot tears, which are marked as black collar in the micrographs. It is seen that the hot tears exist in interdendritic region, which is expected and explained in previous section. In addition, in case of N-1, white band is observed in the micrograph which corresponds to less solute containing zone; negative macro-segregation.

3. Thermo-mechanical modeling

3.1 Standard thermomechanical modeling

In the standard thermomechanical modelling approach [1,2], the mushy zone (composed of liquid and solid phases) is considered as a homogenized continuum so that a unique velocity field is solved for. The numerical simulation is based on the thermomechanical stress/strain analysis. It is conducted using the 3D finite element code THERCAST. The thermal problem and the mechanical problem are solved sequentially at each time increment. First, the energy conservation is solved on all domains taking into account heat exchange between them. In this resolution, the solidification path is defined a priori. Second, the mechanical problem is solved. The alloy is modelled with a hybrid constitutive equation. Over the solidus temperature, the alloy is seen as a non-Newtonian fluid obeying a temperature-dependent viscoplastic multiplicative law, as follows:

$$\bar{\sigma} = K\left(\sqrt{3}\right)^{m+1} \dot{\bar{\varepsilon}}^{m} \tag{2}$$

where $\bar{\sigma}$ is the equivalent von Mises stress, K the viscoplastic consistency, $\dot{\bar{\varepsilon}}$ the generalized strain rate and m the strain rate sensitivity. The value of m over the liquidus temperature is equal to 1 (Newtonian fluid). Note that the liquidus viscosity is defined as 10 Pas, for numerical stability reasons. Below the solidus temperature, the alloy obeys an elastic viscoplastic constitutive equation, expressed by:

$$\bar{\sigma} = \sigma_y + K\left(\sqrt{3}\right)^{m+1} \bar{\varepsilon}^{n} \dot{\bar{\varepsilon}}^{m} \tag{3}$$

in which σ_y is the plastic yield stress, $\bar{\varepsilon}$ the cumulated plastic strain and n the strain hardening coefficient. Physical properties and constitutive parameters are temperature dependent and determined with experimental data.

Concerning predefined solidification path, to evaluate the effect on hot tearing sensitivity, three paths are used for this type of simulation; one is based on lever rule approximation (LR), meaning that thermodynamic equilibrium is achieved in all existing phases at given temperature. Second is the partial-equilibrium approximation together with the para-equilibrium approximation (PE+PA) in which an interstitial element; i.e. carbon has finite diffusivity in all phases, whereas substitutional elements are frozen in solid phases. In addition, the model can account for peritectic reaction, taking place in the steel grade in Tab. 1, under para-equilibrium condition. Last one is the measurement result by means of unidirectional solidification experiment. The details are explained in reference [6]. The simulation of LR and PE+PA has been performed with Thermo-Calc and the TQ-interface [7] using TCFE6 database [8]. The comparison of solidification paths are shown in Fig. 3.

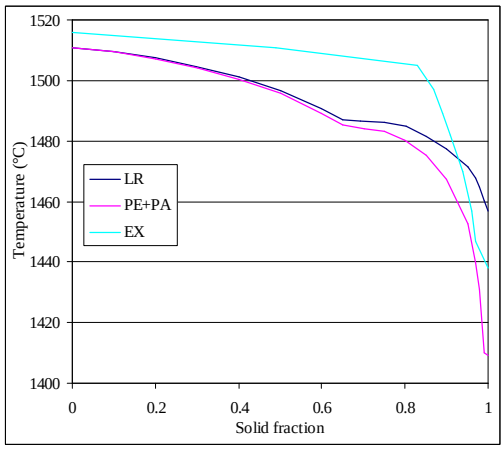

Fig. 3 Comparison of solidification paths; LR: calculated solidification path based on lever rule approximation, PE+PA: calculated solidification path based on partial- and para-equilibrium approximation, EX: measurement result by mean of unidirectional solidification experiment.

As illustrated in Fig. 1, the 3D model is prepared with a consideration of symmetry; half of the setup is modelled. The initial mesh size of the ingot is 8 mm constant and the number of elementis is approximately 600,000. For better accuracy in the bending region, remeshing is performed to obtain finer mesh (4 mm) just before bending, leading to 1,000,000 elements. Filling stage is not taken into account for so that the thermo mechanical simulation starts at 70 s from the start of filling. Concerning the initial temperature of the ingot, uniform temperature as 1550 °C, which is estimated using measurement data, is defined on the ingot domain. For other domains, 20 °C is the initial temperature. The thermal boundary condition in between ingot and mould is defined as air gap dependent heat resistance. When the ingot contacts the mould, the heat transfer coefficient is used as 850 $W/m^2/K$ which is calibrated with measurement results. When air gap generates, the air gap width is considered and the heat exchange depends on radiation between ingot and mould surface and heat conduction in the air, which depends on the gap width. Regarding the ingot top, powder is put after the end of filling. Thus, adiabatic condition is used for the top. After mould removal, the free surface heat exchange is defined as radiation and convection, where the emissivity is taken as 0.8 and the heat transfer coefficient for convection is assumed as 15 $W/m^2/K$.

3.2 "Two phase" modeling and macrosegregation analysis

The second approach is an effective "two phase" modeling in which the liquid and solid velocity fields are computed separately in the mushy zone. It allows simulating solute transport phenomena leading to macro-segregation induced by deformation, shrinkage and advection. It is performed with the 2D finite element code R2SOL. Details of the formulation can be found on reference [4]. The assumptions are listed as follows:

- ✓ The liquid phase is considered as an incompressible Newtonian fluid.
- ✓ The solid phase is seen as a compressible non-Newtonian generalized fluid..
- ✓ The momentum interaction between solid and liquid is taken into consideration with an isotropic Darcy law.
- ✓ Shrinkage term is considered by a different specific mass for liquid and solid phases (ρ_S and ρ_L). However, these are constant in solidification interval.
- ✓ Local thermal equilibrium holds within representative element volume (REV); $T=T_l=T_s$.
- ✓ Simply, a binary alloy system is extended to a multi component system under lever rule approximation, meaning that partition coefficient k_i and liquidus slope m_i are constant for each solute element i.

The above mentioned assumptions lead to the set of conservation equations, expressed as follows:

$$\nabla \cdot \boldsymbol{\Sigma}^s - g_s \nabla p_l + g_l{}^2 \mu_l \kappa^{-1} (\mathbf{v}_l - \mathbf{v}_s) + g_s \rho_s \mathbf{g} = 0 \tag{4}$$

$$\nabla \cdot \left\langle \mathbf{s}^l \right\rangle - g_l \nabla p_l - g_l{}^2 \mu_l \kappa^{-1} (\mathbf{v}_l - \mathbf{v}_s) + g_l \rho_L \mathbf{g} = \rho_L \frac{\partial (g_l \mathbf{v}_l)}{\partial t} + \rho_L \nabla \cdot ((g_l \mathbf{v}_l) \times \mathbf{v}_l) \tag{5}$$

$$\nabla \cdot (g_l \mathbf{v}_l) + \frac{\rho_S}{\rho_L} \nabla \cdot (g_s \mathbf{v}_s) = \left(\frac{\rho_L - \rho_S}{\rho_L} \right) \frac{\partial g_s}{\partial t} \tag{6}$$

$$\langle \rho \rangle \frac{\partial \langle h \rangle}{\partial t} + \nabla \langle h \rangle \cdot \langle \rho \mathbf{v} \rangle + L \nabla \cdot \left(f_l f_s \langle \rho \rangle (\mathbf{v}_l - \mathbf{v}_s) \right) - \nabla \cdot \left(\langle \lambda \rangle \nabla T \right) = 0 \tag{7}$$

$$\frac{\partial \langle w_i \rangle}{\partial t} + \nabla \cdot \left(\langle w_i \rangle \mathbf{v}_s \right) + \nabla \cdot \left(g_l w_{l,i} (\mathbf{v}_l - \mathbf{v}_s) \right) - \nabla \cdot \left(g_l D_l \nabla w_{l,i} \right) = 0 \tag{8}$$

in which $\mathbf{v}_s$ and $\mathbf{v}_l$ are the solid and liquid velocity vector, p_l is the liquid phase pressure, $<\rho>$ and $<\lambda>$ are the average density and the average heat conductivity of the solid and liquid mixture, $<h>$ is the average enthalpy of the mixture. f_s and f_l are respectively the solid and liquid mass fraction, defined as $g_k\rho_k/<\rho>$ with each phase k. $<w_i>$ and $w_{l,i}$ are respectively the average solute concentration and the liquid phase concentration for solute component i. In the momentum equations, the Darcy term is seen with the permeability κ, deriving from liquid phase volume fraction and predefined secondary dendrite arm spacing (Carman-Kozeny model). Constitutive models for the liquid and the solid phases can be seen in reference [4]

Concerning solidification path, it is not defined a priori since solute concentration varies due to solute transport. To model the microsegregation phenomena, we simply extend binary alloy system under lever rule approximation to multi component system. Therefore, constant partition coefficient k_i and liquidus slope m_i for each solute component are assumed. Considering the average enthalpy, one obtains the following relations:

$$T = T_m + \sum_i \left(m_i w_{l,i} \right) \tag{9}$$

$$\langle w_i \rangle = w_{l,i} g_l + (1 - g_l) w_{s,i} = [g_l + (1 - g_l) k_i] w_{l,i} \tag{10}$$

$$\langle h \rangle = c_p T + f_l L \tag{11}$$

where T_m is melting temperature of pure iron, c_p is a constant heat capacity and L is the latent heat. Defining the number of solutes as N_S, the number of equations is N_S+2. <h> and $<w_i>$ are known since these variables are obtained thanks to the global energy and solute conservation resolutions. So, the unknowns are T, g_l and $w_{l,i}$; the number of unknowns is N_S+2. Thus, the set of equations is completed and solved iteratively.

This effective two phase modeling is applied to the case of N-1, in which the ingot centre is fully mushy state during bending. The calculation is carried out in two steps. At first, a standard thermo mechanical calculation is conducted up to just before bending stage. The simulation is then restarted using the "two phase" model. It is assumed that there is no macro segregation at that time.

4. Results and discussion

4.1 Standard thermomechanical simulation result

4.1.1 Temperature evolution in case of N-4

Fig. 4 shows the comparison of temperature evolution in the ingot. There are two thermo couples in the ingot; one is close to the ingot center as blue collar in the schematic in Fig. 4, while another is located in the close to the narrow surface of the ingot. TC-2 shows less solidification time than TC-1 because it is close to the narrow surface but also the surface of the ingot. So, solidification is preceded, compared to TC-1. The calculated result is in good agreement with measurement data, especially during bending.

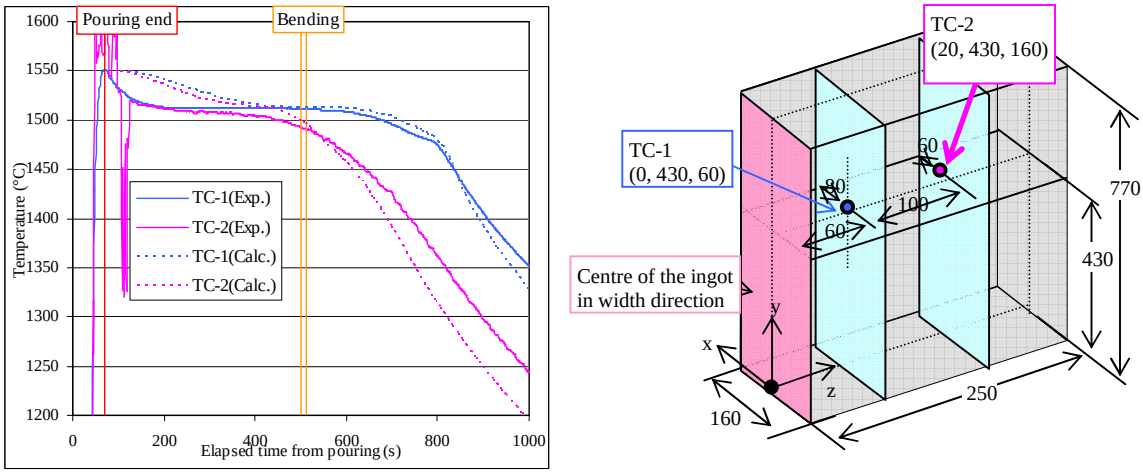

Fig. 4 Comparison of temperature evolution in the ingot (left) and a schematic of thermocouple positi ons in the ingot (right). There are two thermocouples, denoted TC-1 and TC-2. TC-1 is close to the center of the ingot, while TC-2 is close to the narrow surface.

Fig. 5 (left) shows the comparison of surface temperature evolution at the bending tool height. Looking at the calculated result, one can see the change of the evolution at 300 s. At that moment, the mould located in front of the bending tool is removed, prior bending. Consequently, the cooling rate is decreased and the surface temperature is then increased. The calculated temperature evolution is in good agreement with the measured data. So it is concluded that the thermal modeling regarding the boundary condition and thermo physical parameters are well calibrated.

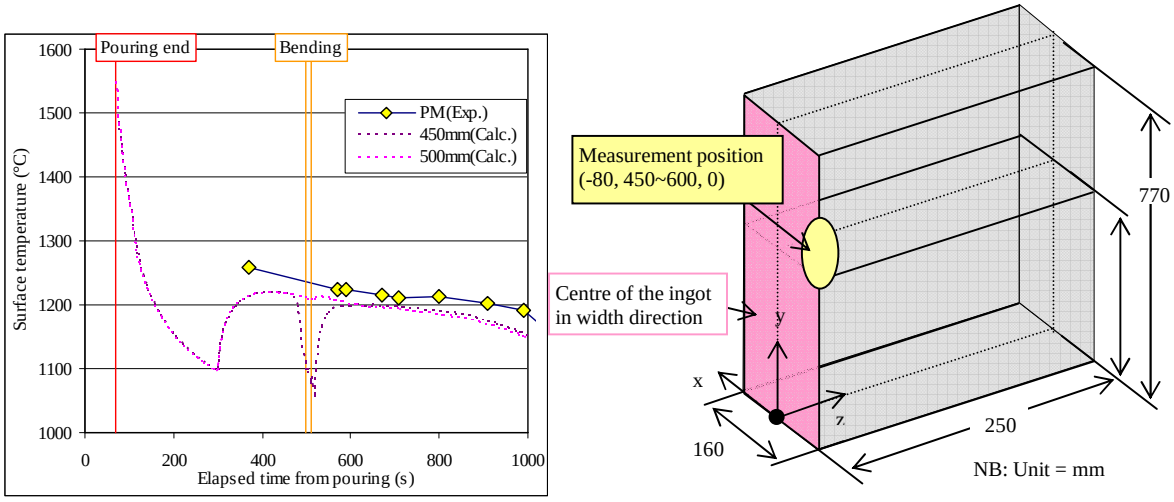

Fig. 5 Comparison of ingot surface temperature evolution (left) and a schematic of measurement position in the ingot surface (right). The measurement has been performed after mould removal.

4.1.2 Hot tearing sensitivity

Fig. 6 demonstrates hot tearing sensitivity field in horizontal section at bending tool height after bending in case of N-4. A positive band can be seen in front of the bending tool. It is in good agreement with the micrograph shown in Fig. 6 where hot tears are observed in the similar position.

Fig. 7 shows the comparison of hot tearing sensitivity profile and cumulated strain profile as a function of the distance from the ingot surface together with the hot tear location from the micrograph. First remark is that the calculated profiles are in good agreement with the measured crack position. The solidification path effect on the location of the high risk is slightly different from each other; in case of LR, the peak is close to the core, while in case of PE+PA, it is located near the surface. The second is the difference of the magnitude of the sensitivity; especially LR case shows lower value than others. It is associated with the difference of BTR. BTR are 17.2 °C, 57.3 °C and 44.5 °C respectively for LR, PE+PA and EX. When BTR is small, the strain limit $\hat{\varepsilon}_C$ is increased and the hot tearing sensitivity is then decreased. The magnitude of the cumulated strain is almost the same in three cases (Fig. 7 (right)) so that the difference of hot tearing sensitivity is directly linked to the difference of BTR.

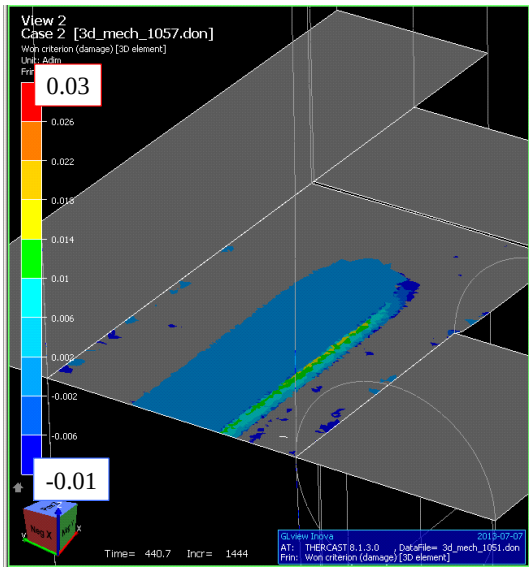

Fig. 6 Hot tearing sensitivity field in horizontal section at the bending tool height with the microsegregation model PE+PA. One can find a positive band along lateral direction in front of the bending tool.

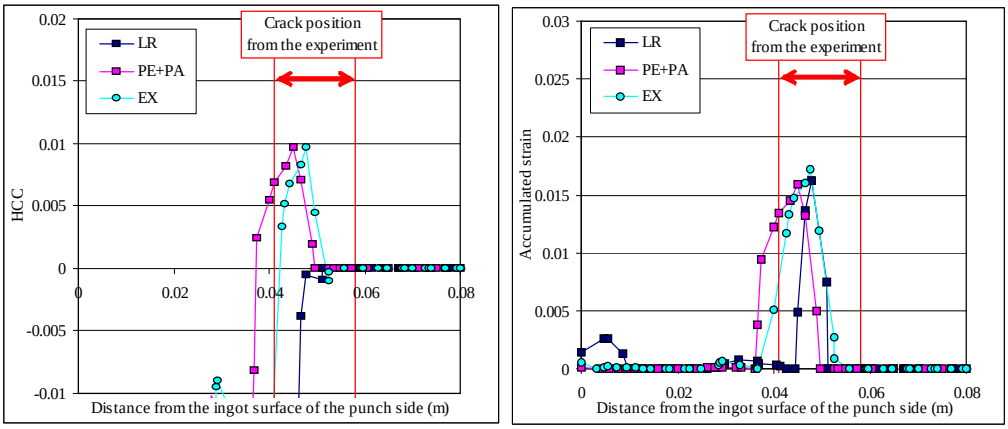

Fig. 7 Comparison of hot tearing sensitivity profile (left) and cumulated strain profile (right) superimposd with hot tear location from the micrograph in case of N-4. Hot tearing sensitivity field in horizontal section at the bending tool height with the microsegregation model PE+PA. One can find positive band along lateral direction in front of the bending tool.

4.2 "Two phase" simulation result

4.2.1 Velocity field during bending

Fig. 8 shows the relative velocity vector field with liquid fraction field during bending. Liquid flow is from the centre to the top, the bottom but also the periphery region because of the compression of the mushy solid phase. It is explained in Fig. 9 that the divergence of solid velocity is negative at the centre. Regarding the periphery region, tensile deformation along the vertical direction takes place so that liquid flow turns to the periphery in order to conserve mass.

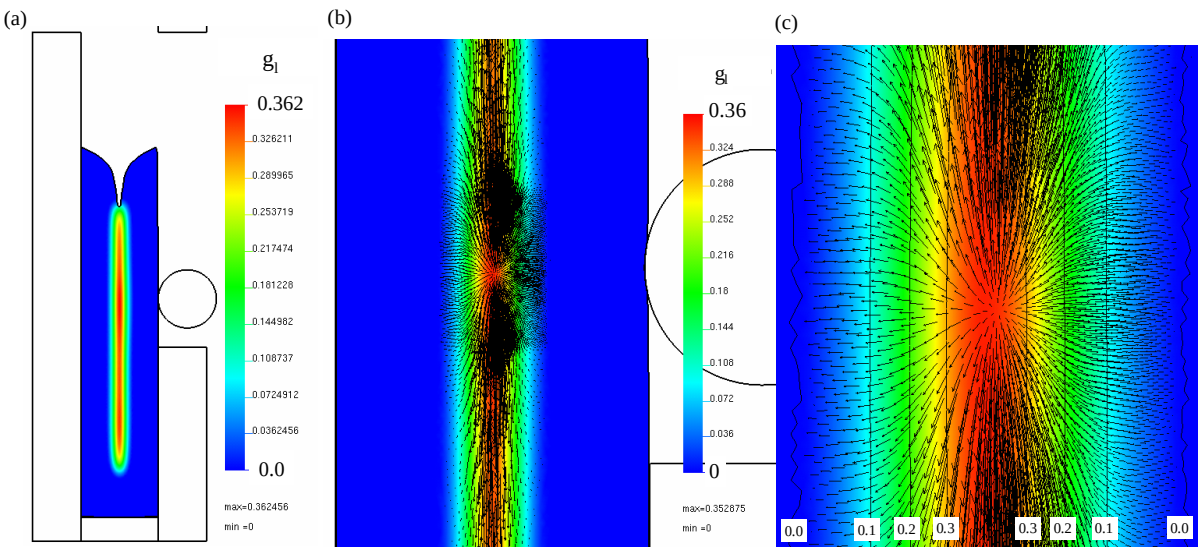

Fig. 8 Liquid fraction field before 2 phase simulation restart (a), liquid fraction field with relative velocity vector (v_l - v_s) during bending (b) and (c). (c) is close to the bending region with liquid fraction isotherms as eight vertical black lines.

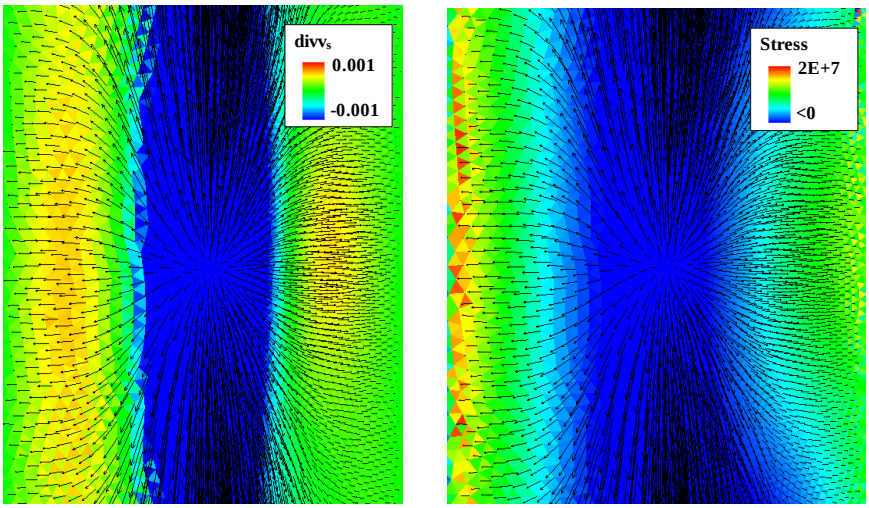

Fig. 9 Divergence of v_s field with relative velocity vector (left). Due to the compression of mushy solid, the centre shows negative values. In contrast, the periphery shows positive values, meaning expansion. It is verified by the right figure where the positive vertical stress is presented. It is seen that the tensile stress generates on the periphery region along the vertical direction. As a consequence, liquid flow turns to the periphery.

4.2.2 Solute concentration field

Calculated relative solute concentration field is presented in Fig. 10. Because of the relative velocity field discussed at the previous section, negative segregation is created at the centre of the ingot and the positive segregation generates at the top, the bottom and the periphery. Concerning bending region, the calculated negative segregation is in good agreement with the white band position in the micrograph. Note that the white band indicates less solute elements. Since the partition coefficient is less than 1.0 in both cases (k_{Mn} = 0.70, k_P = 0.28), macro-segregation pattern is similar but the magnitude is different; P favors segregation as expected. On the periphery, positive concentration can be seen but the magnitude is quite small. Therefore, macro-segregation may not have a big impact on hot tearing sensitivity. For better discussion, quantitative comparison is useful and it is in progress now.

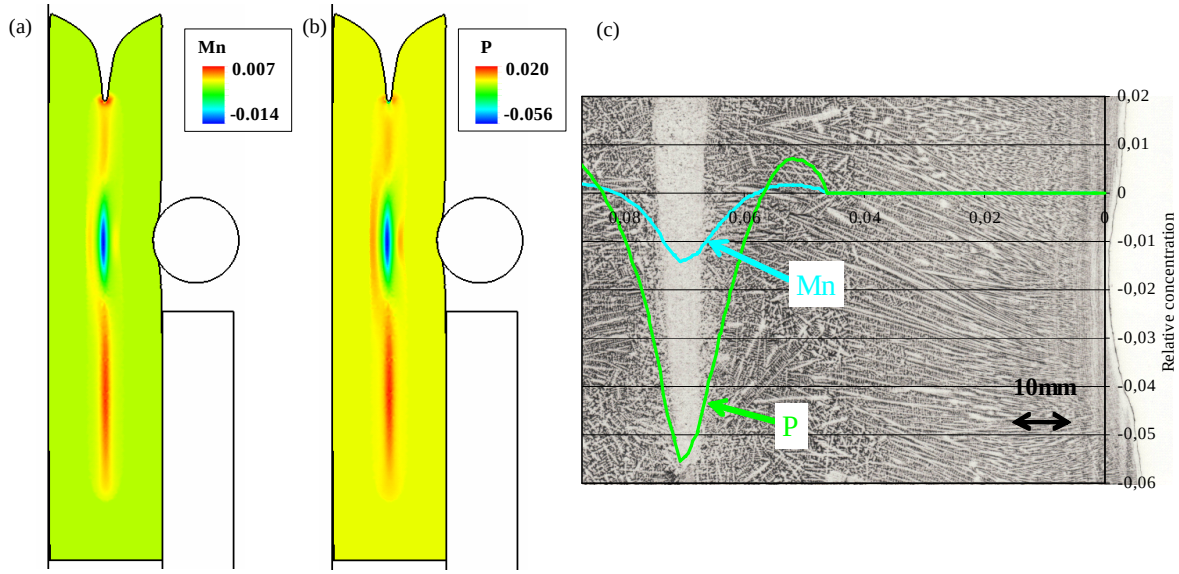

Fig. 10 Relative concentration field after bending; (a) is Mn, (b) is P. (c) is a comparison of calculated relative concentration profile at the bending tool height along horizontal direction with the micrograph. The position of the calculated negative concentration peak is in good agreement with the white band in the micrograph which indicates less solute elements. Note that relative solute concentration is defined as $(\langle w_i \rangle - w_0)/w_0$.

(4) Contribution of convection, shrinkage and solid phase compression on macrosegregation formation

Now, the volume average mass conservation equation (Eq. (6)) is introduced to the volume average solute conservation equation (Eq. (8)). In addition, the time derivative of solute and solid fraction decomposed into a time derivative with respect to the mesh, whose velocity is $\mathbf{v}_s$, and an advection term are employed, leading to:

$$\frac{\partial_{msh}\langle w_i\rangle}{\partial t} = -\nabla w_{l,i}\cdot\left(g_l\left(\mathbf{v}_l-\mathbf{v}_s\right)\right)+\nabla\cdot\left(g_l D_l \nabla w_{l,i}\right)+w_{l,i}\left(\frac{\rho_S-\rho_L}{\rho_L}\right)\frac{\partial_{msh} g_s}{\partial t}+\left(w_{l,i}\frac{\langle\rho\rangle}{\rho_L}-\langle w_i\rangle\right)\nabla\cdot\mathbf{v}_s \qquad (14)$$

The first term of the second member is linked to convection, the next is diffusion, the third is shrinkage and the last is solid phase compression. In order to understand each contribution to macrosegregation formation, four calculations have been conducted in which only one term is accounted for respectively; for instance, the convection term is tested where other terms are deactivated. The results are summarized in Tab. 2. As expected, solid phase compression is dominant for the formation of macrosegregation.

Tab. 2 Summary of each term contribution to macrosegregation with respect to P relative concentration ($(<w_i> - w_{i,0})/w_{i,0}$ [%])

	Convection	Diffusion	Shrinkage	Solid phase compression
Ingot centre	˜ 0 %	˜ 0 %	+0.3 %	+6 %
Periphery	-0.3 %	˜ 0 %	˜ 0 %	+1 %

5. Conclusions

An ingot bending test has been modeled by two numerical codes. Using a standard thermomechanical model, it is then found that strain based criteria have a capability to predict crack occurrence. In addition, micro-segregation model has an impact on hot tearing sensitivity, as expected. Through effective “two phase” simulation, it is demonstrated that negative segregation generates at the centre of the ingot mainly due to solid phase deformation, which is observed in the cast ingot. Quantitative comparison with respect to solute concentration is in progress and the first results should be available soon. Also, all experiments are being modeled and the results will be discussed soon.

Acknowledgement

This work has been supported by Nippon Steel & Sumitomo Metal Corporation in a collaboration project with ArcelorMittal. The authors are deeply grateful to Dr. O. Jaouen and Dr. F. Costes, from Transvalor SA, for their kind help and discussion about thermomechanical modeling using THERCAST software.

Literature

[1] BELLET M, JAOUEN O, POITRAULT I, 2005 *Int. J. Num. Meth. Heat Fluid Flow* **15** 120

[2] BELLET M, FACHINOTTI V. D, 2004 *Comput. Meth. Appl. Mech. Eng.* **193** 4355

[3] BELLET M, CERRI O, BOBADILLA M, CHASTEL Y, 2009 *Mater. Trans.* A **40** 2705

[4] FACHINOTTI V.D, LE CORRE S, TRIOLET N, BOBADILLA M, BELLET M, 2006 *Int. J. Num. Meth. Eng.* **67** 1341

[5] WON Y. M, YEO T. –J, SEOL D. J, OH K. H, 2000 *Mater. Trans.* B **31** 779

[6] KOSHIKAWA T, GANDIN C.A, BELLET M, YAMAMURA H, BOBADILLA M, 2014 *ISIJ* (Abstract has been submitted)

[7] Thermo-Calc TCCS manuals Thermo-Calc software AB (Stockholm, SE), (2013)

[8] P. Shi: TCS steels/Fe-alloys database V6.0 Thermo-Calc Software AB (Stockholm, SE), (2008)